Original Research

Symmetry of the Fornix Using Diffusion Tensor Imaging

Uta N. Sboto-Frankenstein, PhD,[1,2,3]* Tiffany Lazar, BSc,[2] R. Bruce Bolster, PhD,[2,3] Sunny Thind, BSc,[3] Patricia Dreessen de Gervai, MD,[3] Marco L.H. Gruwel, PhD,[3,4] Stephen D. Smith, PhD,[2,3] and Boguslaw Tomanek, PhD[1,5,6]

Purpose: To: 1) Present fornix tractography in its entirety for 20 healthy individuals to assess variability. 2) Provide individual and groupwise whole tract diffusion parameter symmetry assessments prior to clinical application. 3) Compare whole tract diffusion parameter assessments with tract-based spatial statistics (TBSS).

Materials and Methods: Diffusion tensor imaging (DTI) data were acquired on a 3T Siemens magnetic resonance imaging (MRI) system using a single-shot spin echo planar imaging (EPI) sequence. Individual fornix tractography was conducted and whole tract diffusion parameter symmetries assessed. Whole tract results were compared with asymmetry contrasts conducted with voxelwise statistical analysis of diffusion parameters using TBSS.

Results: The fornix tract could be visualized in its entirety including the columns, body, crura, and fimbria. Contrary to the crus and body, there were some tractography inconsistencies of the columns and fimbria across subjects. Although whole tract diffusion parameter asymmetries were nonsignificant, fractional anisotropy (FA) values bordered on statistical significance ($P = 0.052$). Using TBSS, significant FA asymmetries were identified ($P \leq 0.01$, corrected).

Conclusion: The findings demonstrate consistency of fornix tractography as well as some variability in the columns and fimbria. While parametric assessment demonstrates diffusion parameter symmetry, permutation-based TBSS analysis reveals significant FA asymmetries in the crura and fimbriae.

Key Words: fornix; diffusion tensor imaging; tractography; asymmetry; TBSS
J. Magn. Reson. Imaging 2014;40:929–936.

IN THE 1950s the functional significance of the fornix, a brain white matter (WM) connecting the hippocampus with the mammillary bodies, septal nuclei, and nucleus accumbens, remained obscure (1,2). The fornix, together with the hippocampus, is part of the Papez circuit (3), a neural network underlying memory and emotive processes that can be compromised by fornix damage or pathology (4–8).

Fornix WM fibers constitute the main efferent fiber system of the hippocampal formation. The tract is composed of axons of cells in the subicular cortex and pyramidal cells of the hippocampus which spread over the ventricular surface as the alveus and converge to form the fimbria (1). Reaching the posterior aspect of the hippocampus, the fimbriae arch under the splenium of the corpus callosum as the crura and travel beneath the corpus callosum converging at midline to form the body of the fornix. The body of the fornix continues anteriorly towards the anterior commissure where it turns ventrally in front of the interventricular foramina and once again separates bilaterally to form the columns (1).

The complete visualization of the fornix using diffusion tensor imaging (DTI) tractography and the assessment of *whole* tract diffusion parameters are complicated by its small size, curved trajectory, and proximity to cerebrospinal fluid (CSF) (9–14). DTI is a magnetic resonance (MR) technique that is sensitive to the diffusion of water molecules. In brain, WM tracts diffusion is directionally dependent and thus anisotropic (15). This technique allows virtual tract dissection and the assessment of WM by providing diffusion properties for particular tracts of interest (16,17). Since significant tractography and diffusion parameter asymmetry might be taken to reflect unilateral pathology, it is important to know

[1]Alberta Innovates Technology Futures, MR Technology, Winnipeg, MB, Canada.
[2]Biopsychology Program, Department of Psychology, University of Winnipeg, Winnipeg, MB, Canada.
[3]National Research Council Institute for Biodiagnostics, MR Technology, Winnipeg, MB, Canada.
[4]National Research Council Aquatic and Crop Resource Development, Winnipeg, MB, Canada.
[5]Department of Oncology, University of Alberta, Edmonton, AB, Canada.
[6]Multimodal and Functional Imaging Group, Central Europe Institute of Technology, Brno, Czech Republic.
Contract grant sponsor: Manitoba Health Research Council; Contract grant sponsor: Natural Sciences and Engineering Research Council of Canada.
*Address reprint requests to: U.S.-F., Magnetic Resonance Technology, Alberta Innovates Technology Futures, 435 Ellice Ave., Winnipeg, MB R3B 1Y6, Canada. E-mail: UtaFrankenstein@sboto.com
Received April 2, 2013; Accepted August 30, 2013.
DOI 10.1002/jmri.24424
View this article online at wileyonlinelibrary.com.

what degree of asymmetry exists in the normal population.

Generally, fornix diffusion parameters are reported as symmetrical (10,14,18), but anatomical and diffusion asymmetries have been documented in particular segments of the tract (10,13,19). Tractography and diffusion parameter symmetry reports have largely focused on particular segments of the fornix involving mostly the body, or the body with combinations of the crura and/or column segments (9,10,12,18).

The current study has three primary objectives: 1) Present complete fornix tractography and corresponding diffusion parameters for 20 individual datasets to assess commonalities and individual differences. 2) Provide whole tract diffusion parameters including fractional anisotropy (FA), mean diffusivity (MD), axial (AD) and radial diffusivities (RD) for each subject and the group as a whole enabling the assessment of hemispheric asymmetries. 3) Use TBSS to test for local asymmetries that might not emerge in the whole tract results. We hypothesized that complete visualization of the fornix including columns, body, crura, and fimbria can be achieved at 3T and that diffusion parameters are symmetric.

MATERIALS AND METHODS

Subjects

Twenty neurologically healthy volunteers (10 males, mean age 22.5 ± 2.66, range 19–30; all right-handed) participated in the study. The Ethics Committees of the National Research Council of Canada and the University of Winnipeg approved the study and all participants were recruited by posters placed at the University of Winnipeg and paid for their participation. All participants completed MR safety screening and gave informed, written consent prior to entry into the magnet.

MR Data Acquisition

Data were collected at the National Research Council Institute for Biodiagnostics. A whole-body 3T clinical Siemens (Erlangen, Germany) TIM-TRIO MRI scanner with a 12-channel phased array head matrix coil was used. Whole brain anatomical images were acquired in the sagittal plane using a magnetization prepared rapid gradient echo (MP-RAGE) spoiled gradient-echo sequence with the following parameters: one slab with 176 slices and a 0.5 mm gap, slice thickness: 1 mm, in-plane resolution: 1.0 × 1.0 mm, TR/TE: 1900/2.2 msec, flip angle: 9°, acquisition matrix: 256 × 256, field of view (FOV): 240 mm.

DTI data were acquired using a single-shot spin echo planar imaging (EPI) sequence. Imaging was performed using the following scanning parameters: imaging plane: axial, phase encoding direction: anterior–posterior; echo spacing: 0.82 msec, TE: 93 msec, TR: 9100 msec; number of slices: 66, interslice gap: 0 mm; bandwidth: 1396 Hz/pixel, voxel size: 1.9 × 1.9 × 1.9 mm; acquisition matrix: 128 × 128, NEX: 4. Images were acquired with b values of 0 and 1000 s/mm^2 in 20 directions following an icosahedral scheme. Parallel acquisition using a generalized autocalibrating partially parallel acquisition with an effective acceleration factor of 2 was used for an acquisition time of 13 minutes 13 seconds.

Data Analysis

Preprocessing and analysis of diffusion data began with the conversion of DICOM images into a 4D Nifti file and corresponding bvecs and bvals using MRIcron (20). Correction for eddy currents and simple head motion was performed using the FDT module of the FSL Software Library (FMRIB Centre, University of Oxford, Oxford, UK) (21). These eddy current and motion-corrected files were used for tractography in MedINRIA 1.90 (Medical Image Navigation and Research Tool by INRIA, Sophia Antipolos, France; http://www.sop.inria.fr.asclepios/software/-MedINRIA) (22,23) and Tract Based Spatial Statistics (TBSS) (FMRIB Software Library 4.1, http://www.fmrib.ox.ac.uk/fsl) (24).

Region of Interest Selection and Tractography

Individual tractography and subsequent diffusion parameter measurements were performed separately for the right and left fornix in each subject. Regions of interest (ROIs) were selected based on anatomical knowledge of the fornix and its fiber projections. Within each hemisphere, inclusion ROIs were placed at two distinct portions of the fornix in the axial plane. The first dorsal inclusion ROI was placed around the crura of the fornix where the fusion of the left and right tracts is visible. The second ventral inclusion ROI encompassed the fornix at the level of the top of the cerebral peduncles and narrowed the inclusion of streamlines to only those that passed through both ROIs 1 and 2. ROIs were placed in this way to track the right and left sides of the fornix separately. Exclusion ROIs were placed to eliminate streamlines that were clearly not part of the fornix. All analyses for fiber tracking used MedINRIA default values. Minimal streamline length was set to 10 mm, the smoothness of reconstructed streamlines to 20, and the threshold to initiate tracking was FA $\geq$0.3.

Whole Tract Diffusion Parameter Statistical Analysis

Mean whole tract (left or right) FA and eigenvalues (λ_1, λ_2, and λ_3) were determined. Using the three eigenvalues, axial (AD = λ_1), radial (RD = $(\lambda_2+\lambda_3)/2$) and mean diffusivities (MD = $(\lambda_1+\lambda_2+\lambda_3)/3$) were calculated. Paired difference *t*-tests were carried out with SPSS 14.0 (Chicago, IL) (25) to compare diffusion parameter measurements between the left and right hemispheres. We also assessed the effect of sex on diffusion parameter asymmetries. Results are reported as significant if they had a P value ≤ 0.05.

Tract-Based Spatial Statistics

Voxelwise statistical analysis of the FA, MD, AD, and RD data was carried out using TBSS. First, FA images were created by fitting a tensor model to the raw

diffusion data using FDT, and then brain-extracted using BET (26). All subjects' FA data were then aligned to Montreal Neurological Institute (MNI) 152 space using the nonlinear registration tool FNIRT (27), which uses a b-spline representation of the registration warp field (28), Next, the mean FA image was created and thinned to create a mean FA skeleton which represents the centers of all tracts common to the group. Each subject's aligned diffusion parameter (FA, MD, AD, RD) data were then projected onto this skeleton and the resulting data fed into voxelwise cross-subject statistics.

In order to test skeleton voxels on the left of the fornix vs. those on the right, a symmetric mean FA skeleton, mask, and distance map were generated. The 4D prealigned data (all_FA) were then projected onto the symmetrized skeleton. The resulting 4D all_FA_symmetrized_skeletonized file was left–right tested (the same steps were repeated for MD, AD, and RD all_symmetrized-skeletonized files). To test for R>L we inverted the data and reran the "randomize" script.

Statistical Analysis

Voxelwise analyses of the asymmetry images were performed using permutation-based, voxelwise nonparametric testing (as implemented in the randomize tool, part of FSL) (29). The Threshold-Free Cluster Enhancement (TFCE) option was used to avoid the need for setting an arbitrary initial cluster-forming threshold. The resulting TFCE *P*-value images were fully corrected for multiple comparisons across space. We also assessed the effect of sex on diffusion parameter asymmetry. Significance levels for *t*-tests (two-tailed) were set at $P = 0.05$, corrected for multiple comparisons across space (voxel-level inference). The number of permutations was 5000. The anatomical location of significant fornix voxels was determined with reference to the ICBM-DTI-81 white-matter labels atlas provided by FSL (30).

RESULTS

Figure 1 presents the directionally encoded tractography of the fornix for every dataset of the 20 subjects who participated in the study. The tractography shows that the fornix can be visualized in its entirety (columns, body, crura, and fimbriae) using 1.9 mm isotropic voxels and 20 gradient directions at 3T. Table 1 presents the whole tract diffusion parameters for the tracts depicted in Fig. 1. None of the whole

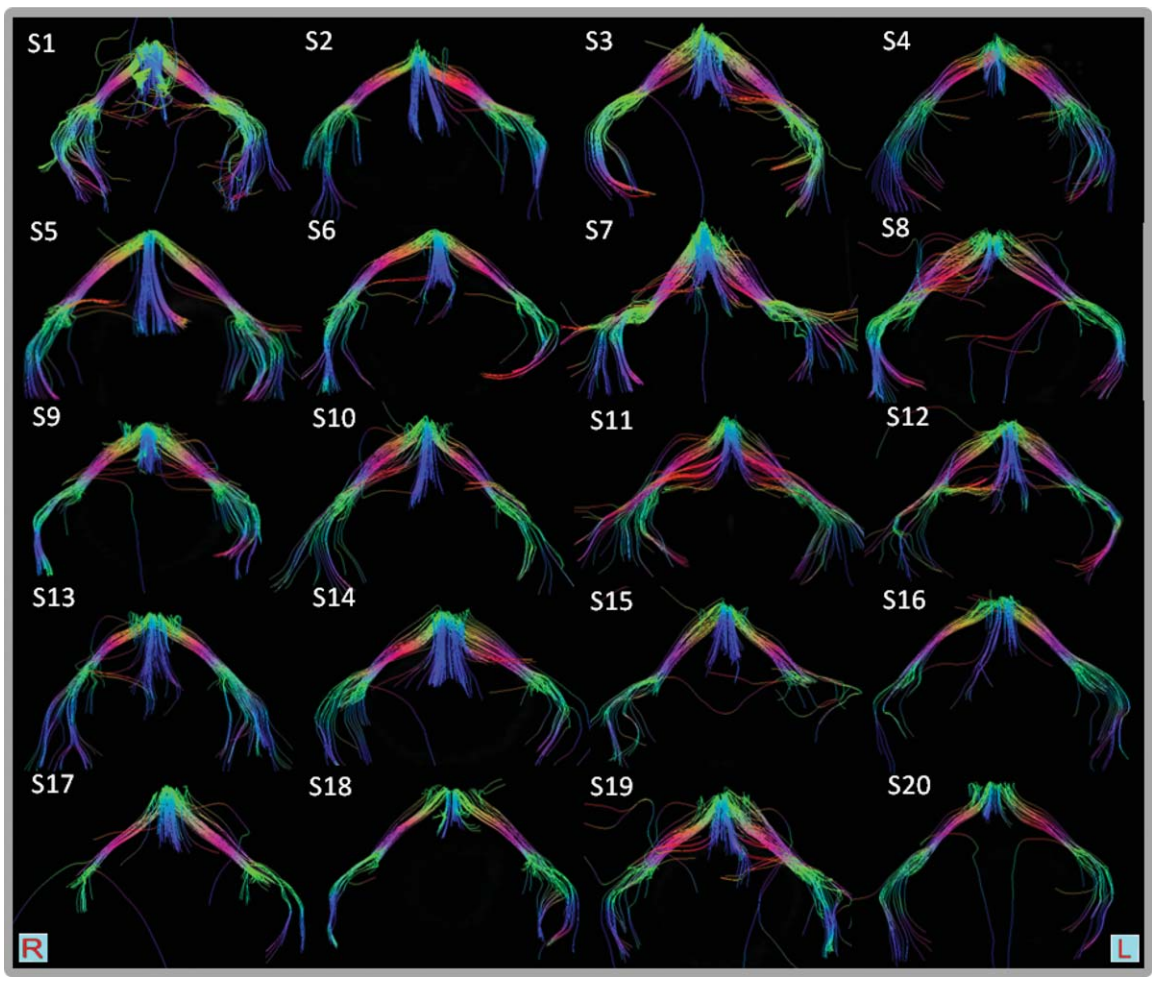

Figure 1. Fornix tractography in 20 individual subjects. All tracts are depicted in an anterior view in coronal plane. The left side of the tract is on the right side of the image and the right side of the tract is on the left side of the image. DEC FA tracts are presented for every subject. DEC coding corresponds to red: left–right, green: anterior–posterior and blue: inferior–superior.

Table 1
Mean Whole Tract Diffusion Parameters of the Fornix (x 10 ^{3} mm^{2}/sec)

	Right		SD	Left		SD	*P*-value
FA	0.33	±	0.17	0.34	±	0.17	0.052
MD	1.12	±	0.55	1.11	±	0.56	0.838
AD	1.50	±	0.60	1.50	±	0.62	0.871
RD	0.93	±	0.52	0.92	±	0.53	0.629

tract diffusion parameters demonstrate significant asymmetries, although the FA value asymmetry approaches significance ($P = 0.052$). Figure 3 shows FA asymmetries in the left crus and fimbria of the fornix, the only significant diffusion parameter asymmetry obtained with TBSS. Neither the male/female whole tract diffusion parameter *t*-tests nor the male/female TBSS contrasts reached statistical significance.

Tractography

Figure 1 shows that the directionally encoded tractography is consistent with known anatomical features of the fornix, and reproducible in 20 subjects. The columns, body, crura, and fimbriae are all well represented. In all subjects the columns trek in a ventral–dorsal direction (blue). There are some subjects (S9, 17, 18, 20) where the columns appear truncated and/or not clearly separated into two separate streamline bundles. In all subjects the columns join at the body of the fornix which moves anterior–posterior (green) until it separates laterally into the left and right crura (red). The crura are well tracked and arch laterally (red) from the body of the fornix into the fimbriae and are clearly visible in every subject. The crura arch in a ventro–anterior direction into the fimbria (green) of the fornix, which travel towards the head of the hippocampus where they branch ventrally (blue) and fan out. Two subjects (S15, 17) show truncated fimbriae in one hemisphere at this most anterior aspect of the tract.

Figure 2 shows a representative example (S1) of an FA intensity encoded fornix. The figure also shows the individual right and left fornix tracts that were used for all diffusion parameter asymmetry assessments, depicted in sagittal perspective, as well as the two tracts combined and viewed in the coronal plane. The FA intensity encoded map shows a distinct distribution of FA values along the tract. While lower FA values (purple-blue) are seen in the columns, lateral aspects of the body and in the fimbria (particularly where they branch ventrally at the head of the hippocampus), the highest FA values (yellow-orange-red) are seen in the medial aspect of the body of the fornix and the crura (green-yellow). This pattern of FA value distribution along the tract is uniform in all 20 subjects.

Whole Tract Diffusion Parameters

Table 1 presents average whole tract diffusion parameter values for the left and right fornix for the group. Diffusion parameter values were consistent between subjects and hemispheres. Because we are reporting whole tract values, standard deviations for left and right *whole* tract diffusion parameters in individual subjects were high. Differences in FA approached significance for the comparison between the left and right ($P = 0.052$) fornix. By comparison, the paired sample *t*-tests indicated that there were no significant laterality differences in axial ($P = 0.871$), radial ($P = 0.629$), and mean ($P = 0.838$) diffusivities.

Tract-Based Spatial Statistics

Significant FA asymmetries were observed in two segments of the fornix ($P \leq 0.01$). The largest difference was observed in the left crus (x = −24 y = −33 z = 1) followed by the left fimbria (x = −30 y = −13 z = −12). Figure 3a depicts increased FA in the left crus of the fornix relative to the right. Figure 3b displays increased FA in the left fimbria relative to the right.

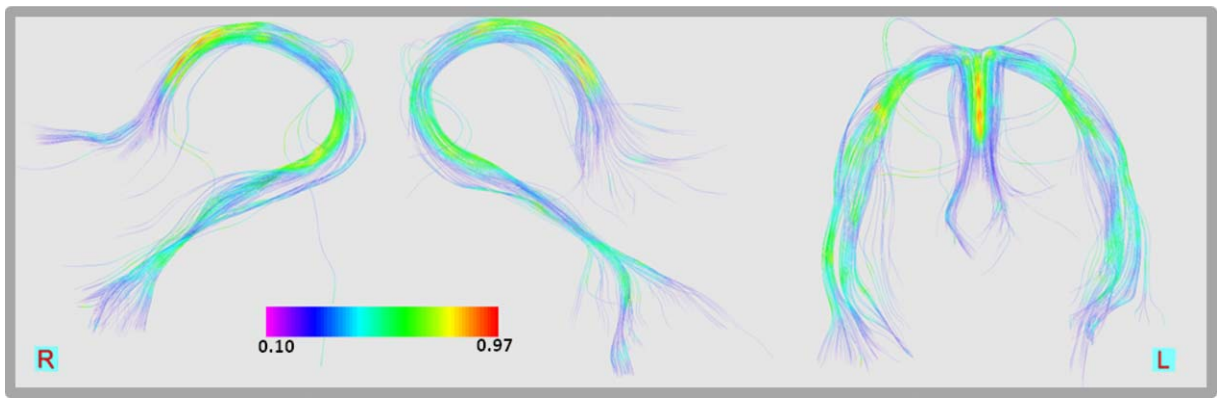

Figure 2. The figure shows an FA-intensity coded map in a representative subject (S1). The individual right and left fornix tracts are depicted in sagittal perspective, as well as the two tracts combined and viewed in the coronal plane. The FA intensity coding demonstrates that FA is highest in the body and crura of the fornix and lowest in the columns and small branching fibers of the fimbria at the anterior aspect of the hippocampus. This characterization of FA intensities is representative of the consistent path and distribution of FA values along the tract from subject to subject. FA values are higher in areas of low fiber branching (body, cura) and lower in areas of high fiber branching (columns and anterior aspect of the fimbria). [Color figure can be viewed in the online issue, which is available at wileyonlinelibrary.com.]

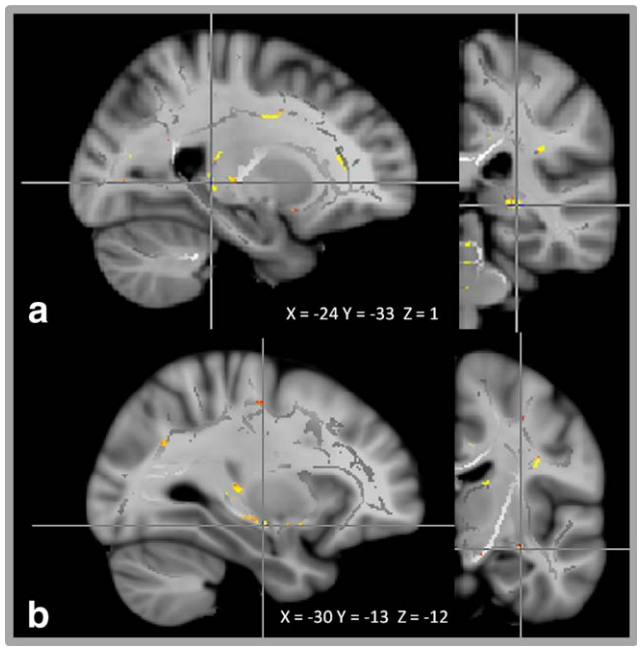

Figure 3. TBSS of L>R demonstrates significant differences in segments of the fornix including the crus (**a**, crosshairs) and fimbria (**b**, crosshairs). For better anatomical reference the crus and fimbria of the fornix are shown in sagittal and coronal planes. Significant L>R FA differences are overlaid on the symmetrized FA skeleton (grayscale) and the MNI 152 background anatomical image provided by FSL. [Color figure can be viewed in the online issue, which is available at wileyonlinelibrary.com.]

The cluster maximum depicted by the crosshair in Fig. 3b (particularly in the coronal slice) appears to locate to an area superior to the fornix fimbria. This crosshair location is examined in the limitations of our methods below. None of the other diffusion parameter contrasts demonstrated significant asymmetries, consistent with the whole-tract-based analyses.

DISCUSSION

The results support our hypothesis and demonstrate that tractography of the fornix in its entirety including the columns, body, crura, and fimbriae is feasible and reproducible at 3T. Depiction of all and not just one representative subject is important to assess the degree of consistency across subjects and provides a more comprehensive understanding of tract features unique to individuals. Initially, analyses of whole tract diffusion parameters revealed values that appeared generally lower than those reported in previous studies; potential factors contributing to these results are discussed below. Although FA asymmetries approached significance in the whole tract analyses, only TBSS demonstrated significant laterality differences in the crura and fimbriae, demonstrating that TBSS is a more sensitive tool to detect local FA asymmetries.

Tractography

The fornix tractography conducted in the present study is comparable to that presented for a representative subject by Catani et al (16,17). By contrast in the current study, we present individual directionally color-coded tractography for 20 datasets (20 fornix tracts). Major features are consistent across subjects. All subjects consistently show the fimbria traveling posteriorly from the hippocampus and parahippocampal gyrus, the crura arching dorsal and medial towards the body of the fornix, and the body orienting anterior at midline below the body of the corpus callosum. The two columns are visible as two streamline bundles projecting ventrally.

However, it is important to show that there were minor aspects that varied across subjects, primarily at the ends of the tract, including both columns and fimbria. This is important in clinical decisions as to how "typical" the fornix might be for a particular individual.

Even though the individual columns cannot be seen as two separate streamline bundles in some subjects, the majority of subjects demonstrate a clear separation of the left and right columns. The columns were also clearly visualized by Catani et al (16,17) and depicted in one representative subject. Using a standard axial T_2-weighted anatomical image, Supprian and Hofmann (13) were able to distinguish between the two columns of the fornix in the majority of subjects with the left column located caudal to the right, but the authors were unable to detect both columns in 9 of 63 subjects. Thus, there is convergence between the current DTI experiment and also those based purely on anatomical imaging. While fornix columns have been well visualized using tractography at 1.5T (16–18), another 3T study (12) reports the visualization of the columns in every one of their 30 subjects. Once again, however, the results are only presented for one representative subject. In that subject, the anterior dorsal/ventral extent of the columns is not well visualized. The tract is not directionally encoded and it is therefore difficult to determine if the columns were completely tracked in the anterior dorsoventral extent in the remaining subjects. Another study (9) conducted at 3T reports an 80% visualization of the pars tecta (columns) of the fornix. Again, the columns are depicted in one representative subject, the tract is not directionally encoded, and even with high resolution isotropic voxels, column streamline visualization in that one representative subject is limited.

With the exception of Catani et al (16,17) and Mori et al (30) at 1.5T and Metzler-Baddeley et al (11) at 3T, there are fewer DTI studies fully depicting the fimbriae of the fornix. In the current study the fimbria appeared unilaterally truncated at their most anterior aspect for two subjects (S15, 17). Nevertheless the complete bilateral fimbria segments were clearly tracked in 95% (38/40) of the tracts examined. This is in comparison to a reported 83% visualization rate of the fimbria (9) and no report of fimbria visualization at 3T (12).

Contrary to some studies (9,12,18), where the crura were more difficult to visualize using standard DTI, we had a 100% success rate tracking this segment of the fornix. Apart from the body, the crus was the

most consistent feature identified in our tractography. Okada et al (12) reported that the left crus was visualized in 90% of their subjects, and the right crus in 70%. By comparison, we were able to track right and left crura in 100% of our subjects. Thus, we suggest that the results of Okada et al (12) reflect incomplete tractography as opposed to genuine individual differences.

Diffusion Parameters

Assessment of FA and MD values reveals results that compare with some studies, but differ from others in certain respects. At first glance the tabled fornix FA values presented in our study appear lower than those reported by others (9,10,14,18). Fujiwara et al (9) used high-resolution DTI at 3T, with a voxel size comparable to ours and reported mean fornix FA values of 0.41. Similarly, Yasmin et al (14) presented mean FA values of 0.41 in the fornix of their youngest age group. Upon closer examination of the regions of interest used in both studies, it can be seen that the diffusion parameters were average values derived from voxels primarily in the body of the fornix. Fujiwara et al (9) showed representative high-resolution fornix tractography where the body of the fornix is more completely tracked relative to the columns and fimbria. Yasmin et al (14) derived their diffusion parameters from the voxelized core of the fornix, a region analogous to the body of the fornix where FA values are high relative to other regions of the tract (18,31). Since FA values in our study are derived from an average of the voxels of the entire tract, including columns and fimbria, where FA values are low, our overall tract FA values are lower than those reported by Fujiwara et al (9) and Yasmin et al (14). To compare our diffusion parameter values more directly to those studies, we performed targeted manual ROI FA assessments in the body of the fornix in all subjects at the point where the crura converged (results not included in the table). As the data would predict, we observed a comparable average FA value of 0.45 at this ROI relative to an average FA value of 0.33 in the whole tract assessments.

Proximity of the fornix to the third and lateral ventricles can degrade signal resolution due to partial voluming from inclusion of voxels containing CSF. Concha et al (18) used FLAIR to minimize signal attenuation from CSF. This resulted in a significant FA increase averaged over the body, crura, and columns of the fornix and a significant decrease in mean apparent diffusion coefficient (ADC) in the same segment. By contrast, Metzler-Baddeley et al (11) implemented a postacquisition free water elimination approach to minimize the contribution of CSF contamination, and report FA values similar to ours and those reported by others (6,9,14,32). None of these studies report fornix FA values close to 0.5. In the study by Concha et al (18) the use of standard DTI resulted in voxels belonging to the top portion of the crus suffering from partial volume averaging and dropping below the anisotropy threshold (0.3), resulting in incomplete tractography of the crus. In the current study we were able to generate a complete fornix including the top portions of the crura without the application of CSF suppression. Thus, lower FA values in our study are not due to incomplete tractography; however, further studies are warranted to assess the impact of CSF signal suppression on diffusion parameters at 3T.

Whole tract MD measurements of 1.12 for the right and 1.11 for the left fornix in our study are also lower than measurements obtained in some studies (9,14) but comparable to those reported by others (18,32). Yasmin et al (14) report MD values of 1.66 and 1.73 for the right and left body of the fornix and Fujiwara et al (9) report mean ADC values of 1.40. Both of these studies include older subject groups (mean ages of 58 and 51 years). Therefore, lower MD values in our younger subject cohort (mean age of 22.5 years) are consistent with the observation that age-related degradation of WM results in loss of tissue organization and changes in water diffusivity which are reflected in increased MD values. The mean age in Concha et al's subject group (18) (mean age of 28 years) is comparable to the mean age of our subject group. Mean ADC values (when averaged across segments) reported in that study closely resemble our whole tract MD measurements and thus further support previous studies demonstrating that higher MD values are seen in older subject populations (14,32).

FA A/Symmetry

None of our whole tract diffusion parameters demonstrated significant asymmetry (Table 1). However, comparison of whole tract FA values for left greater than right differences yielded results that approached, but did not reach, statistical significance. The lack of diffusion parameter asymmetry has also been reported by others. Yasmin et al (14), who assessed the core (body) of the fornix, reported no asymmetry in FA and MD. Malykhin et al (10), who assessed the crura of the fornix, report no significant FA asymmetries, but a 4.5% increase of trace ADC in the left crus. Concha et al (18) did not detect any significant asymmetries for FA and mean ADC in the crus, body, and columns of the fornix, and thus present data collapsed over the left and right fornix. Recently, a large TBSS study (33) documented whole-brain WM FA asymmetries; however, fornix asymmetries were not reported. Upon closer inspection of the figures, FA asymmetries favoring the right fornix can be observed ($z = 16–20$ mm). The authors discuss the potential influence of genetics, environmental factors, and race on WM asymmetry and it is of interest to note that FA asymmetry favors the left fornix in our comparably small Caucasian subject group. The current TBSS results also confirm that while the fornix body is symmetrical with respect to FA (14,18), leftward asymmetries appeared in the more distal regions of the tract, specifically the crus and fimbria. While symmetry has been reported for FA in the body and crura (10,18), leftward FA asymmetry in the crus and fimbria has not. The TBSS results can also help explain the nonsignificant FA results in the whole tract analysis,

given the inclusion of the symmetric high FA values in the body of the fornix. Hence, the results of this study demonstrate that TBSS is a more sensitive method in identifying FA differences in specific segments of the fornix.

Limitations and Technical Considerations

A limitation of the DTI technique is that the resolution of the anatomical detail of the fornix tractography is inferred from the path of least resistance to water diffusion and thus only approximates the anatomical reality of WM microarchitecture. Furthermore, the complexity of axonal fiber architecture within a voxel can include linear, crossing, and kissing fibers and the assumption of a single fiber population per voxel is inadequate to capture this complexity. High angular resolution imaging (HARDI) techniques have been developed to address this limitation (34).

Postprocessing tractography algorithms can be divided into deterministic (streamline) and probabilistic methods. The fornix tractography in this study was conducted with deterministic tractography, which uses the principal direction of the first eigenvector to reconstruct WM tracts, but cannot account for uncertainty or for distributed connectivity. However, deterministic tractography remains the most commonly used technique clinically (35). Probabilistic tractography estimates a probability distribution of each fiber direction in a voxel and thus accounts both for the uncertainty in the data and for the possible existence of multiple fiber directions within each voxel. However, the probabilistic approach is slower and therefore cannot be used interactively in the clinic. Not deflating the strength of the technique, it is harder to interpret visually (35). Instead of distinct streamline visualization, probabilistic methods provide volume maps of probable connectivities, necessitating more timely and knowledgeable anatomical interpretation and making it less efficient for clinical applications.

TBSS is also less applicable for clinical evaluations. TBSS is time-consuming and the ability to identify WM differences unique to individuals is lost in the generation of a WM skeleton common to the group. Furthermore, the depiction of the exact location of particular segments of the fornix using the cluster maximum has to be evaluated with care: 1) Our cluster maximum for the fornix fimbria was identified as the fornix/stria terminalis by the JHU ICBM-DTI-81 atlas and our method was not able to distinguish between these two tracts. 2) The cluster maximum crosshair points to an area that appears to be superior to the fornix fimbria and localize more closely to the tail of the caudate, underlining that crosshair location, cluster maximum, and anatomical identification have to be interpreted with caution.

Due to its proximity to periventricular regions, the fornix is highly susceptible to CSF contamination-based partial volume effects. In addition to FLAIR, a free water elimination approach can be applied post-hoc to minimize CSF partial volume effects (11,36). Nonetheless, we show that good tractography can be obtained without CSF suppression using sequences and analytic tools that are available in most clinical settings.

Axial and radial diffusivity measurements are reported in Table 1. Axial diffusivity is the principal eigenvalue of the diffusion tensor and radial diffusivity is the average of the second and third eigenvalues. While axial and radial diffusivities have been used to reflect axonal and myelin integrity in healthy white matter (37), the use of these parameters in the characterization of pathological tissue has been recently discouraged unless accompanied by a thorough investigation of their mathematical and geometrical properties (38).

There are a number of factors that impact the signal-to-noise ratio (SNR) which in turn affects tractography and diffusion parameters. Magnetic field strength, the sequence used, the strength of the gradients and the number of gradient directions, the type of coil, the voxel size, and the use of parallel imaging all contribute to the results obtained in this study. Although a thorough review of all of these factors is beyond the scope of this study (see Mukherjee et al (39) for review), some of these methodological aspects deserve further consideration. It has been demonstrated that the stability and accuracy of DTI measurements are substantially higher at 3T relative to 1.5T (40). The increase in SNR with field strength can provide higher spatial resolution and higher diffusion weighting, which can improve the accuracy of diffusion studies in the human brain. We calculated the SNR by dividing the mean signal of a selected ROI in the B0 image by the standard deviation of the background noise and obtained an SNR of 83. In addition, we optimized our acquisition parameters by using 20 gradient directions, small isotropic voxels, four averages, and by applying parallel imaging (GRAPPA) to minimize distortions associated with EPI sequences.

In conclusion, a prerequisite in characterizing diffusion parameter asymmetries of the fornix in health and disease is the ability to fully visualize the tract including the columns, body, crura, and fimbriae. Here we demonstrate consistency of tractography between subjects but also highlight intersubject variations in the columns and fimbria in 20 healthy volunteers. Consistent with our hypothesis, whole tract diffusion parameters were largely symmetric. Even though TBSS demonstrates local FA asymmetries in the crura and fimbria of the fornix in the grouped analysis, significant whole tract FA asymmetry in individual subjects may be a clinical indicator of disease.

ACKNOWLEDGMENT

The authors thank Michelle Di Nella for research assistance.

REFERENCES

1. Carpenter M. Core text of neuroanatomy, 4th ed. Baltimore, MD: Williams & Wilkins; 1996.
2. Daitz HM, Powell TPS. Studies of the connexions of the fornix system. J Neurol Neurosurg Psychiatry 1954;17:75–82.

3. Papez JW. A proposed mechanism of emotion. 1937. J Neuropsychiatry Clin Neurosci 1995;7:103–112.
4. Copenhaver BR, Rabin LA, Saykin AJ, et al. The fornix and mammillary bodies in older adults with Alzheimer's disease, mild cognitive impairment, and cognitive complaints: a volumetric MRI study. Psychiatry Res Neuroimaging 2006;147:93–103.
5. Fitzsimmons J, Kubicki M, Smith K, et al. Diffusion tractography of the fornix in schizophrenia. Schizophr Res 2009;107:39–46.
6. Kern KC, Ekstrom AD, Suthana NA, et al. Fornix damage limits verbal memory functional compensation in multiple sclerosis. NeuroImage 2012;59:2932–2940.
7. Onu M, Roceanu A, Sboto-Frankenstein U, et al. Diffusion abnormality maps in demyelinating disease: Correlations with clinical scores. Eur J Radiol 2012;81:386–391.
8. Thomas AG, Koumellis P, Dineen RA. The fornix in health and disease: an imaging review. Radiographics 2011;31:1107–1121.
9. Fujiwara S, Sasaki M, Kanbara Y, Inoue T, Hirooka R, Ogawa A. Feasibility of 1.6-mm isotropic voxel diffusion tensor tractography in depicting limbic fibers. Neuroradiology 2008;50:131–136.
10. Malykhin N, Concha L, Seres P, Beaulieu C, Coupland NJ. Diffusion tensor imaging tractography and reliability analysis for limbic and paralimbic white matter tracts. Psychiatry Res Neuroimaging 2008;164:132–142.
11. Metzler-Baddeley C, O'Sullivan MJ, Bells S, Pasternak O, Jones DK. How and how not to correct for CSF-contamination in diffusion MRI. NeuroImage 2012;59:1394–1403.
12. Okada T, Miki Y, Fushimi Y, et al. Diffusion-tensor fiber tractography: intraindividual comparison of 3.0-T and 1.5-T MR imaging. Radiology 2006;238:668–678.
13. Supprian T, Hofmann E. The fornix of the human brain: evidence of left/right asymmetry on axial MRI scans. Surg Radiol Anat 1997;19:105–109.
14. Yasmin H, Aoki S, Abe O, et al. Tract-specific analysis of white matter pathways in healthy subjects: a pilot study using diffusion tensor MRI. Neuroradiology 2009;51:831–840.
15. Basser PJ, Pierpaoli C. Microstructural and physiological features of tissues elucidated by quantitative-diffusion-tensor MRI. J Magn Reson B 1996;111:209–219.
16. Catani M, Thiebaut de Schotten M. A diffusion tensor imaging tractography atlas for virtual in vivo dissections. Cortex 2008;44:1105–1132.
17. Catani M, Howard RJ, Pajevic S, Jones DK. Virtual in vivo interactive dissection of white matter fasciculi in the human brain. NeuroImage 2002;17:77–94.
18. Concha L, Gross DW, Beaulieu C. Diffusion tensor tractography of the limbic system. AJNR Am J Neuroradiol 2005;26:2267–2274.
19. Lazar T, Thind S, Bolster RB. Whole tract versus tract based spatial statistics assessment of fornix fractional anisotropy. Hum Brain Mapp 2013 [Epub ahead of print].
20. Rorden C, Karnath H-O, Bonilha L. Improving lesion-symptom mapping. J Cogn Neurosci 2007;19:1081–1088.
21. Smith SM, Jenkinson M, Woolrich MW, et al. Advances in functional and structural MR image analysis and implementation as FSL. Neuroimage 2004;23(Suppl 1):S208–219.
22. Fillard P, Arsigny V, Pennec X, Ayache N.Clinical DT-MRI estimation, smoothing and fiber tracking with log-Euclidean metrics. In: 3rd IEEE International Symposium on Biomedical Imaging: Nano to Macro; 2006. p 786–789.
23. Fillard P, Penne X, Arsigny V, Ayache N. Clinical DT-MRI estimation, smoothing, and fiber tracking with log-Euclidean metrics. IEEE Trans Med Imaging 2007;26:1472–1482.
24. Smith SM, Jenkinson M, Johansen-Berg H, et al. Tract-based spatial statistics: voxelwise analysis of multi-subject diffusion data. Neuroimage 2006;31:1487–1505.
25. IBM SPSS software, December 17 CT500. Retrieved December 18 2012 from http://www-01.ibm.com/software/analytics/spss/
26. Smith SM. Fast robust automated brain extraction. Hum Brain Mapp 2002;17:143–155.
27. Anderson JLR, Jenkinson M, Smith S.Non-linear optimization. FMRIB technical report TR07JA1. 2007.
28. Rueckert D, Sonoda LI, Hayes C. et al. Non-rigid registration using free form deformations: application to breast MR images. IEEE Trans Med Imaging 1999;18:712–721.
29. Nichols TE, Holmes AP. Nonparametric permutation tests for functional neuroimaging: a primer with examples. Hum Brain Mapp 2002;15:1–25.
30. Mori S, Wakana S, Nagae-Poetscher LM van Zijl. MRI atlas of human white matter, 1st ed. Baltimore, MD: Elsevier; 2005.
31. Concha L, Beaulieu C, Wheatley BM, Gross DW. Bilateral white matter diffusion changes persist after epilepsy surgery. Epilepsia 2007;48:931–940.
32. Zahr NM, Rohlfing T, Pfefferbaum A, Sullivan EV. Problem solving, working memory, and motor correlates of association and commissural fiber bundles in normal aging: a quantitative fiber tracking study. NeuroImage 2009;44:1050–1062.
33. Takao H, Hayashi N, Ohtomo K. White matter asymmetry in healthy individuals: a diffusion tensor imaging study using tract-based spatial statistics. Neuroscience 2011;193:291–299.
34. Tuch DS, Weisskoff RM, Belliveau JW, Wedeen VJ.High angular resolution diffusion imaging of the human brain. In: Proc 7th Annual Meeting ISMRM, Philadelphia; 1999.
35. Yamada K, Akazawa K, Yuen S, Nishimura T. Clinical MR tractography: past, present, and future. MedicaMundi 2009;53:9–15.
36. Pasternak O, Sochen N, Gur Y, Intrator N, Assaf Y. Free water elimination and mapping from diffusion MRI. Magn Reson Med 2009;62:717–730.
37. Song S-K, Sun S-W, Ramsbottom MJ, Chang C, Russell J, Cross AH. Dysmyelination revealed through MRI as increased radial (but unchanged axial) diffusion of water. Neuroimage 2002;17:1429–1436.
38. Wheeler-Kingshott CAM, Cercignani M. About "axial" and "radial" diffusivities. Magn Reson Med 2009;61:1255–1260.
39. Mukherjee P, Chung SW, Berman JI, Hess CP, Henry RG. Diffusion tensor MR imaging and fiber tractography: technical considerations. AJNR Am J Neuroradiol 2008;29:843–852.
40. Alexander AL, Lee JE, Wu Y-C, Field AS. Comparison of diffusion tensor imaging measurements at 3.0 T versus 1.5 T with and without parallel imaging. Neuroimaging Clin N Am 2006;16:299–309, xi.